Linkage between cellular communications, energy utilization, and proliferation in metastatic neuroendocrine cancers

Joseph E. Ippolito*, Matthew E. Merritt†, Fredrik Bäckhed*, Krista L. Moulder‡, Steven Mennerick‡§, Jill K. Manchester*, Seth T. Gammon¶, David Piwnica-Worms¶, and Jeffrey I. Gordon*‖

*Center for Genome Sciences, Washington University, St. Louis, MO 63108; †Advanced Imaging Research Center, Department of Radiology, University of Texas Southwestern Medical Center, Dallas, TX 75390; and Departments of ‡Psychiatry, §Anatomy and Neurobiology, and ¶Molecular Biology and Pharmacology and Molecular Imaging Center, Mallinckrodt Institute of Radiology, Washington University School of Medicine, St. Louis, MO 63110

Contributed by Jeffrey I. Gordon, June 22, 2006

To identify metabolic features that support the aggressive behavior of human neuroendocrine (NE) cancers, we examined metastatic prostate NE tumors and derived prostate NE cancer (PNEC) cell lines from a transgenic mouse model using a combination of magic angle spinning NMR spectroscopy, *in silico* predictions of biotransformations that observed metabolites may undergo, biochemical tests of these predictions, and electrophysiological/calcium imaging studies. Malignant NE cells undergo excitation and increased proliferation when their $GABA_A$, glutamate, and/or glycine receptors are stimulated, use glutamate and GABA as substrates for NADH biosynthesis, and produce propylene glycol, a precursor of pyruvate derived from glycine that increases levels of circulating free fatty acids through extra-NE cell effects. Treatment of nude mice containing PNEC tumor xenografts with (*i*) amiloride, a diuretic that inhibits Abp1, an enzyme involved in NE cell GABA metabolism, (*ii*) carbidopa, an inhibitor of dopa decarboxylase which functions upstream of Abp1, plus (*iii*) flumazenil, a benzodiazepine antagonist that binds to $GABA_A$ receptors, leads to significant reductions in tumor growth. These findings may be generally applicable: GeneChip data sets from 471 human neoplasms revealed that components of GABA metabolic pathways, including ABP1, exhibit statistically significant increases in their expression in NE and non-NE cancers.

metabolome-directed cancer therapy | electrophysiology | GABA signaling and shunt | magic angle spinning-NMR | metabolomics

Neuroendocrine (NE) cancers originate from either neuroectoderm or endoderm-derived epithelia and display a wide range of aggressiveness. On one end of the spectrum, neuroectodermal NE cancers originating from adrenal chromaffin cells (phenochromocytomas) are typically indolent with ≤10% undergoing metastatic spread (1). In contrast, small cell carcinoma, an endodermal NE tumor comprising up to 25% of lung cancers, is usually disseminated at the time of initial diagnosis (2). Adenocarcinomas originating in non-NE cell lineages in the lung, prostate, stomach, and colon, as well as other organs, can express NE cell-associated gene products. This "neuroendocrine differentiation" (NED) correlates with poor prognosis (3–8), although the underlying mechanisms remain obscure.

To characterize the metabolic features of NE cancers and adenocarcinomas with NED that affect prognosis, we produced CR2-large T antigen (TAg) transgenic mice where transcriptional regulatory elements from the mouse cryptidin-2 gene (*Defcr2*) were used to direct expression of simian virus 40 TAg in a subset of prostate NE cells. Males from multiple pedigrees develop metastatic NE cell cancer with a very stereotyped pattern of progression. Transgene expression commences at 7 weeks of age. Within 1 week, foci of transformed NE cells appear that phenocopy human prostatic intraepithelial neoplasia, the postulated precursor of conventional adenocarcinoma of the prostate (9, 10). By 16 weeks of age, there is local invasion of the tumor in 90% of CR2-TAg prostates, with 25% having tumor nodules >3 mm. The majority of mice die by 24 weeks, with transformed NE cells comprising >90% of all cells in their prostates and with metastases in lymph nodes, liver, lungs, and bone.

CR2-TAg tumors and metastases were used to generate prostate NE cancer (PNEC) cell lines. PNEC cells produce prominent neurite-like processes when grown as attached monolayers and express a variety of gene products that are also present in CR2-TAg prostates and metastases. When grown in suspension cultures, they form multicellular aggregates that resemble the neurospheres produced when neural stem cells are cultured on noncoated surfaces (11). Subcutaneous injection of PNEC cells produces rapidly growing tumor xenografts (average doubling time, 7.5 days), whereas intravenous injection results in liver and bone metastases (11).

Previously, we combined GeneChip data sets obtained from CR2-TAg prostates and metastases plus PNEC cells to obtain a "core" NE transcript profile (8). This profile was used to generate an *in silico* reconstruction of the NE cell metabolome, and compared with GeneChip data sets from good and poor prognosis human NE tumors. The results indicated that a distinguishing feature of poor prognosis NE tumors is a glutamic acid decarboxylase 1 (Gad1)-independent pathway for synthesis of GABA that uses the diamine oxidase, amiloride-binding protein 1 (Abp1). Follow-up GC-MS and LC-MS analyses and electrophysiological studies disclosed that PNEC cells synthesized GABA and expressed functional $GABA_A$ receptors on their surface (8). These findings suggested a previously uncharacterized mechanism for cellular signaling in the NE cancer microenvironment.

In this report, we expand our analysis of cellular metabolism in NE cancer by using a generally applicable strategy. Magic angle spinning NMR spectroscopy (MAS-NMR) profiling of metabolites was merged with *in silico* predictions of cellular metabolism from GeneChip data sets. A complimentary approach used *in silico* predictions of possible metabolite biotransformations based upon known features of metabolite structure. Microanalytical biochemical assays were then used to obtain quantitative data about the activities of key enzymes and the levels of specified metabolites. This strategy, combined with electrophysiological studies, led to the discovery that NE cancer cells use molecules involved in cellular communications to increase their stores of available energy and to promote their proliferation. The importance of this paradigm to NE cancer aggressiveness was underscored by a pharmacologic intervention

Conflict of interest statement: No conflicts declared.

Freely available online through the PNAS open access option.

Abbreviations: NE, neuroendocrine; NED, NE differentiation; TAg, large T antigen; PNEC, prostate NE cancer; MAS-NMR, magic angle spinning NMR; TCA, tricarboxylic acid.

‖To whom correspondence should be addressed. E-mail: jgordon@wustl.edu.

that targeted key enzymes and neurotransmitter receptors with well established drugs used for other diseases.

Results and Discussion

Magic Angle Spinning NMR Spectroscopy of NE Cell Metabolites. To identify metabolites indicative of NE cancer, we compared the MAS-NMR spectra of PNEC cells with the spectra of a human prostate cancer cell line derived from the non-NE, luminal secretory epithelial lineage (LNCaP; ref. 12). MAS-NMR has the advantage of being able to directly profile metabolites in intact tissues or cells without a need for prior extraction and/or chromatographic separation. High-speed sample rotation at an axis of 54.7° (the magic angle) relative to the magnetic field removes residual dipolar couplings and averages susceptibility effects, thereby narrowing line widths and enhancing spectral resolution (13, 14).

Comparison of the spectra obtained from PNEC and LNCaP cells showed that NE cancer cells were enriched for GABA (Fig. 1*A*), validating our previous LC/MS studies (8). In addition to GABA, 1,2-propanediol (propylene glycol) was identified as another abundant metabolite (Fig. 1*B*). We subsequently surveyed our transcriptome-based *in silico* reconstructions of PNEC and CR2-TAg prostatic tumor metabolism and discovered that propylene glycol could be produced from glycine via an amiloride binding protein 1 (Abp1)-generated intermediate, methylglyoxal (Fig. 1*C*). Aldehyde reductase (AKR1B, E.C. 1.1.1.21) could then convert methylglyoxal to propylene glycol. The reconstructions also predicted conversion of propylene glycol to lactate (yielding two molecules of NADH) followed by its conversion to pyruvate (1 NADH), and subsequent entry into the tricarboxylic acid (TCA) cycle (Fig. 1*C*).

In rats, propylene glycol produces acute reductions in basal and insulin-stimulated lipogenesis as well as glucose oxidation in adipocytes, plus acute reductions in glucose uptake in skeletal muscle (15, 16). We found that fasting BALB/c nu/nu (nude) mice containing PNEC tumor xenografts exhibited significantly higher levels of serum free fatty acids (FFAs) compared to age- and gender-matched, non-tumor-bearing nude mouse controls maintained on the same diet and housed in the same microisolators (2.16 ± 0.22 mM vs. 1.32 ± 0.09 mM; $n = 5$ animals per group; $P < 0.01$). A direct link between propylene glycol and serum FFA levels was observed when propylene glycol was injected intraperitoneally (1 μmol per g of body weight) into normal nude mice daily for 1 week. Propylene glycol significantly elevated fasting serum FFAs compared to untreated mice (1.80 ± 0.12 mM vs. 1.32 ± 0.09 mM; $n = 5$ animals per group; $P = 0.01$). Although the mechanism that underlies the effect of propylene glycol on FFA levels is unclear, both glucose and insulin tolerance tests established that nude mice with PNEC tumors were not insulin resistant compared to their age- and gender-matched non-tumor-bearing counterparts (data not shown; $n = 5$ mice per group per test).

These findings underscore one distinctive role amine oxidases, such as Abp1, play in NE cell metabolism: by generating propylene glycol from glycine (a known neurotransmitter), it may increase endogenous pools of energy (NADH), as well as secure exogenous sources (fatty acids). We subsequently evaluated the relationship between neurotransmitter production and cellular energetics in two follow-up experiments: one used an approach we named "biotransformation-directed metabolomics;" the other involved electrophysiological studies of PNEC cells.

Biotransformation-Directed Metabolomics. This approach involves *in silico* predictions of possible metabolite biotransformations based on the chemical groups present in a given metabolite, rather than on the enzymes identified as being present in a cell (e.g., from DNA microarray profiling of mRNAs). Given our observations that (*i*) GABA is enriched in PNEC versus LNCaP cells and (*ii*) GABA biosynthesis and signaling are features of poor prognosis human NE cancers (8), we wanted to determine whether this compound was metabolized further by NE cells. The chemical structure of GABA was entered into METEOR biotransformation prediction software (www.lhasalimited.org), and a list of potential metabolites that could theoretically be produced from GABA was generated. One predicted compound was succinate, a component of the TCA cycle. The "GABA shunt" of the TCA cycle is known to exist in plants and neurons

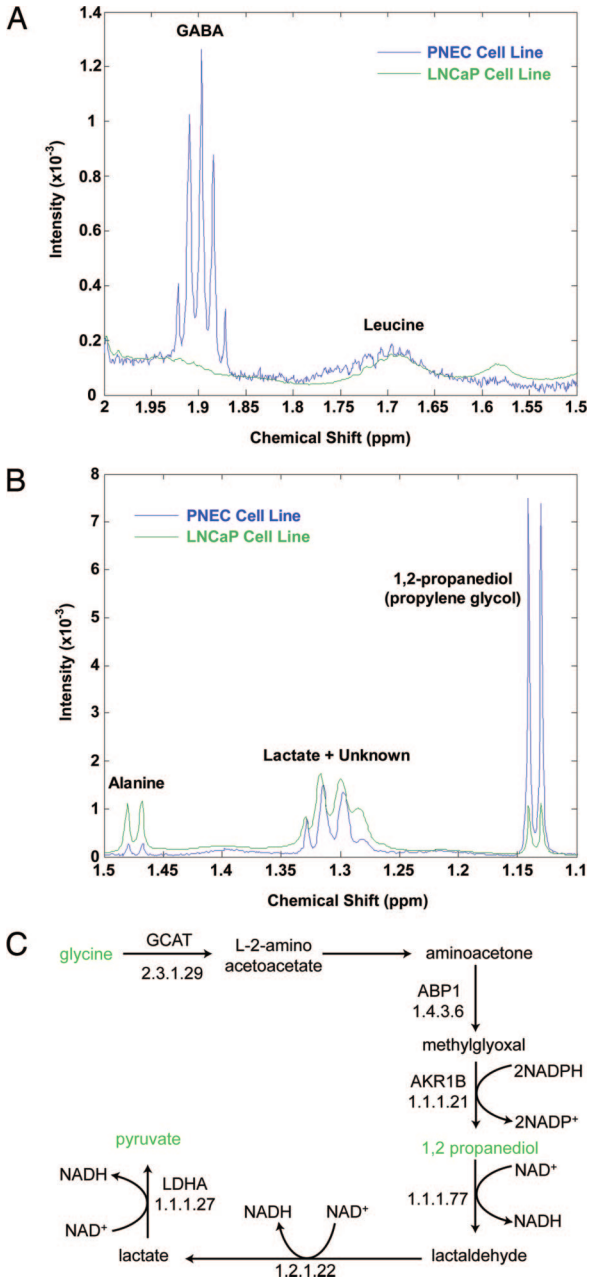

Fig. 1. MAS-NMR spectroscopy studies. (*A*) Spectra were obtained from PNEC and LNCaP cell lines. A portion of the spectrum is shown from 1.5–2.0 ppm, highlighting enrichment of the GABA multiplet in PNEC compared with LNCaP cells. (*B*) Propylene glycol is enriched in PNEC cell lines. Metabolites were identified by proton correlation spectroscopy and by referencing NMR spectral libraries (Chenomx Eclipse software). (*C*) Transcriptome-based *in silico* metabolic reconstruction, showing the predicted pathway for propylene glycol synthesis and metabolism in PNEC cells.

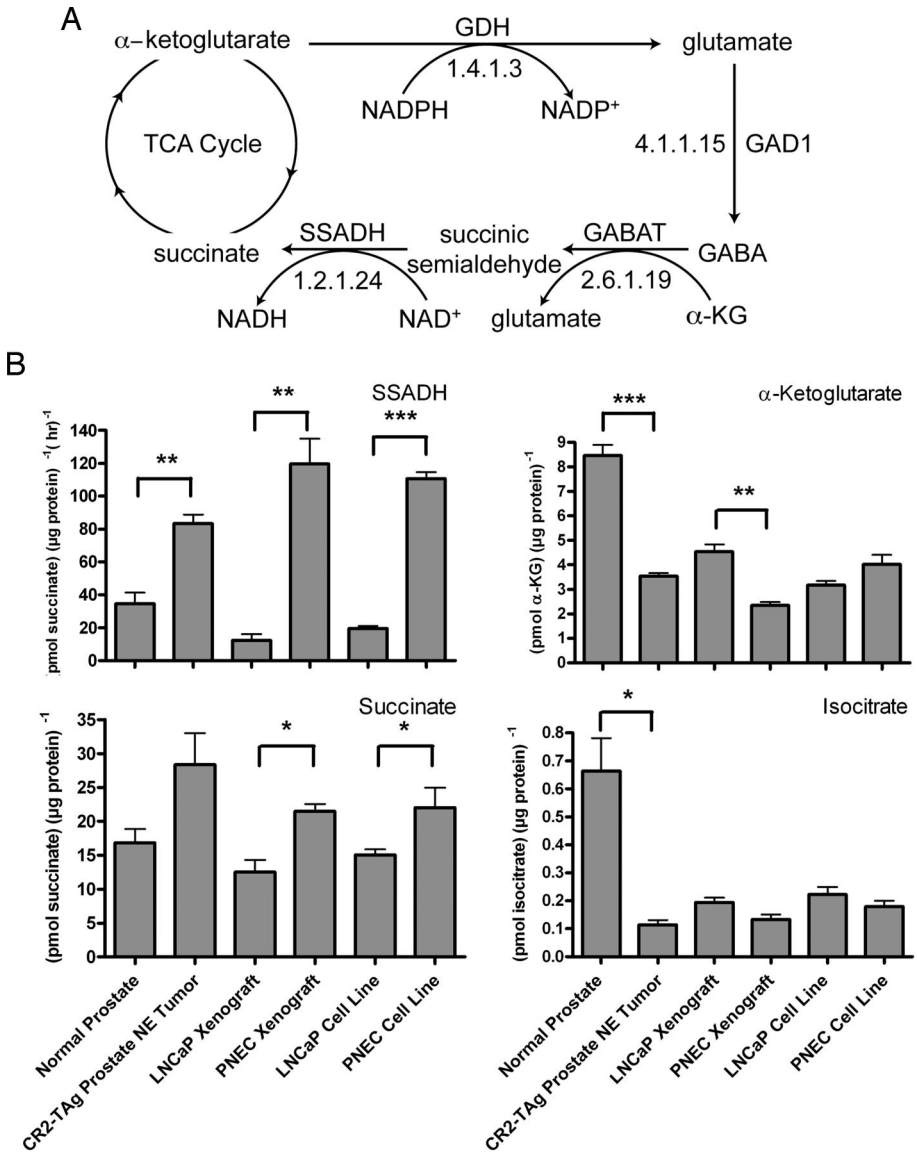

Fig. 2. Evidence for operation of the GABA shunt of the TCA cycle in prostate NE cancer cells. (*A*) Overview of shunt. α-Ketoglutarate is converted to glutamate by glutamate dehydrogenase (GDH), which is converted to GABA by glutamic acid decarboxylase 1 (GAD1). GABA transaminase (GABAT) produces succinic semialdehyde and glutamate from GABA and α-ketoglutarate (α-KG), which is then converted to succinate and NADH by succinic semialdehyde dehydrogenase (SSADH). (*B*) Biochemical assays of GABA shunt components. Bracketed asterisks refer to statistically significant differences between PNEC versus LNCaP cell lines, PNEC versus LNCaP tumor xenografts, or between CR2-TAg prostate NE tumors versus normal prostates (*, $P < 0.05$; **, $P < 0.005$; ***, $P < 0.0005$).

(17, 18). Metabolite flux through this shunt occurs in times of stress or hypoxia, but its physiological significance is unclear (17). An intriguing feature of the shunt is that glutamate, derived from α-ketoglutarate , can give rise to GABA via glutamic acid decarboxylase 1 (Gad1), followed by its conversion to succinic semialdehyde by GABA transaminase, and oxidation of the semialdehyde to succinate by succinic semialdehyde dehydrogenase (SSADH, Aldh5a1), with production of NADH from NAD^+ (Fig. 2*A*). The presence of the GABA shunt would allow the transformed NE cell to store energy in the form of GABA, which can then be reintroduced into the TCA cycle by SSADH, thus producing NADH and $FADH_2$, which can then take part in oxidative phosphorylation.

In silico reconstructions of the metabolome in PNEC cells and CR2-TAg prostate NE tumors, based on assignment of enzyme classification numbers to transcripts detected by GeneChip profiling and placement of these enzymes on KEGG metabolic maps, predicted the presence of a GABA shunt (Fig. 2*A*). To validate these predictions, we performed microanalytic biochemical assays of shunt-associated enzymes and metabolites in cultured PNEC and LNCaP cells, PNEC and LNCaP tumor xenografts, as well as CR2-TAg and normal mouse prostates. Our results support the existence of an active GABA shunt in prostate NE cancer cells: (*i*) PNEC cell lines, PNEC tumors, and CR2-TAg prostates displayed significantly higher SSADH activity than did LNCaP cell lines, LNCaP tumors or normal prostates; (*ii*) α-ketoglutarate, the point of entry into the shunt, was significantly decreased (2-fold; $P < 0.005$) in PNEC versus LNCaP tumors, and CR2-TAg versus normal prostates; (*iii*) succinate, the point of exit from the shunt, was significantly increased (2-fold; $P < 0.05$) in PNEC versus LNCaP cell lines and tumor xenografts; and (*iv*) isocitrate, the precursor of α-ketoglutarate, was not statistically different among any of the cell line or tumor populations (Fig. 2*B*). As an additional control,

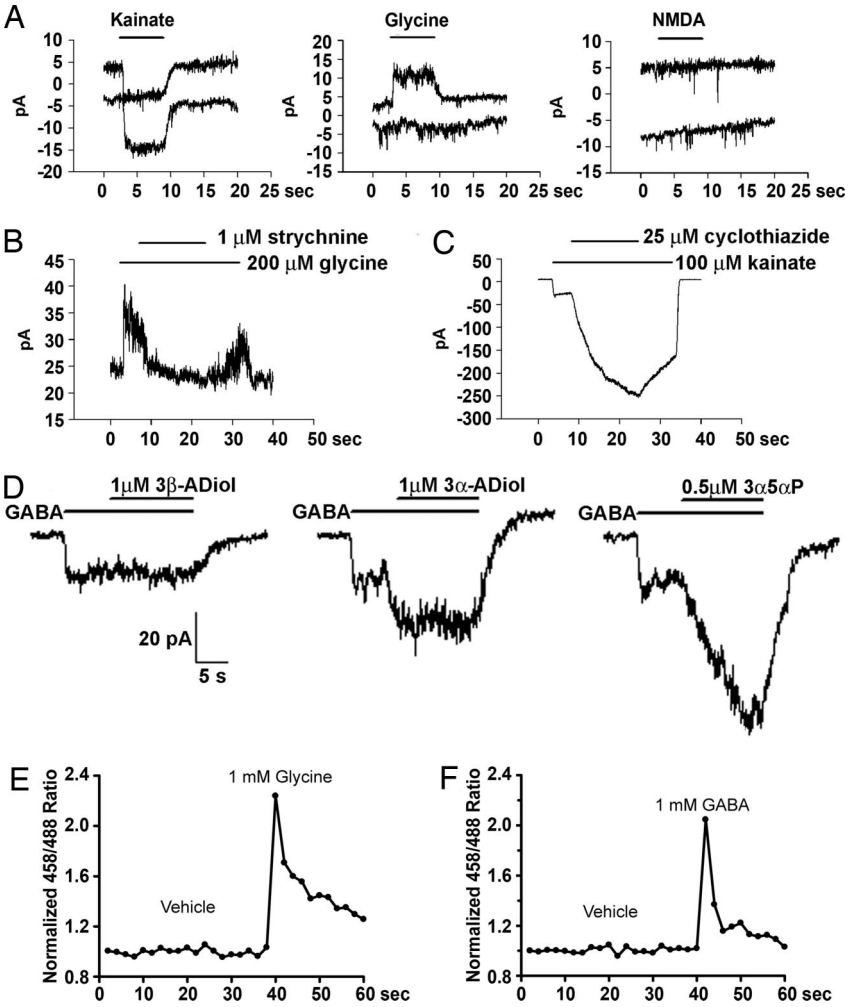

Fig. 3. Electrophysiological characterization and calcium imaging of ligand-induced activity of PNEC cell surface receptors. (*A*) Cellular responses to 50 μM NMDA, 100 μM kainate, and 200 μM glycine. The top trace shows the current response of PNEC cells at −30 mV, whereas the bottom trace is at −60 mV. PNEC cells have functional kainate-activated AMPA/kainate glutamate receptors, but not NMDA receptors. The horizontal bars indicate the duration of exposure to the indicated compounds. (*B*) PNEC cells express strychnine-sensitive glycine receptors. (*C*) PNEC cell ionotropic glutamate receptors are potentiated by cyclothiazide, suggesting activation of AMPA receptors. (*D*) Selective potentiation of $GABA_A$ receptor stimulation by neurosteroids. Metabolic reconstructions of PNEC cells revealed transcripts encoding 17β-hydroxysteroid dehydrogenase type 7 (Hsd17b7), a biomarker of androgen-refractory prostate adenocarcinoma in humans (21) that catalyzes conversion of dihydrotestosterone to 3α-androstanediol and 3β-androstanediol. The neurosteroid 3α-androstanediol (3α-ADiol) potentiates the response, whereas 3β-androstanediol (3β-ADiol) does not. 3α-hydroxy-5α-pregnan-20-one (3α5αP) is used as a positive control. (*E* and *F*) Ratiometric calcium imaging of PNEC cells. Application of glycine (*E*) and GABA (*F*) elicits calcium flux in PNEC cells. Vehicle is modified Earle's balanced salt solution (MEBSS).

we analyzed prostate adenocarcinomas from 32-week-old TRAMP mice ($n = 3$) where T-antigen expression is targeted to the luminal secretory cell rather than to the neuroendocrine cell lineage (19). We found that GABA levels were 44.5-fold higher in PNEC compared to TRAMP tumors (26.7 ± 1.8 vs. 0.6 ± 0.3 pmol per μg of protein, $P < 0.001$). This finding led us to conclude that GABA production is independent of T-antigen expression and a feature of prostate neuroendocrine tumors. Consistent with their lower levels of GABA, we found that SSADH activity was significantly reduced in TRAMP compared to PNEC tumors (67.8 ± 7.8 vs. 392.5 ± 9.7 pmol of succinate per μg of protein per h, $P < 0.001$).

Another metabolic feature of the PNEC cell allows it to add to its NADH reserves. As noted in the Introduction, PNEC cells (and poor prognosis human NE cancers) possess a set of enzymes that allow GABA to be synthesized from putrescine via Abp1- and aldehyde dehydrogenase (Aldh) (8) independent of a Gad1 mediated pathway (Fig. 5, which is published as supporting information on the PNAS web site). GABA synthesis through this alternate route would not have to compete with lipid biosynthesis from acetyl-CoA (TCA cycle precursor), or with production of glutamate from α-ketoglutarate for protein biosynthesis or signaling via glutamate receptors. Moreover, GABA synthesis by Aldh from Abp1-derived 4-aminobutanal produces an additional NADH molecule (Fig. 5) before its conversion to succinic semialdehyde and succinate (which yields yet another molecule of NADH).

Based on these considerations, we assayed NADH and NAD^+ concentrations in PNEC versus LNCaP tumors ($n = 3$ per group). The results confirmed that PNEC tumors had significantly higher NADH levels (0.28 ± 0.01 versus 0.13 ± 0.04 μmol per g of protein; $P < 0.05$), whereas levels of NAD^+ were similar between the two cell lines (1.59 ± 0.45 versus 1.73 ± 0.28 μmol per g of protein).

Signaling via GABA, Glutamate, and Glycine Receptors Stimulates Proliferative Activity in PNEC Cells. $GABA_A$ receptors are ligand-gated chloride ion channels whose function in the mature central

nervous system (CNS) is to hyperpolarize, or inhibit neurons. This function is also shared by glycine receptors, which like $GABA_A$ receptors are ligand-gated chloride ion channels. In the CNS, these receptors are opposed by ionotropic glutamate receptors (20).

When we surveyed GeneChip data sets generated from near confluent monolayers of PNEC cells, CR2-TAg prostate tumors, and normal mouse prostates (http://gordonlab.wustl.edu/metaview/ippolito), we found that, in addition to $GABA_A$ receptor subunits, NE tumor cells are significantly enriched for mRNAs encoding the glycine receptor beta subunit (Glrb) as well as the AMPA2 ionotropic glutamate receptor (Gria2) (reference control, normal prostate; $P < 0.0001$; two-tailed t test). Electrophysiological assays confirmed the presence of functional ionotropic AMPA-type glutamate receptors, based upon their sensitivity to kainate and cyclothiazide, and the presence of glycine receptors, based on their strychnine-sensitive response to glycine (Fig. 3 *A–C*). Interestingly, functional ionotropic NMDA-type glutamate receptors were absent from the cells (Fig. 3*A*), suggesting some selectivity in the expression of membrane ligand-gated channels. These studies also revealed potentiation of $GABA_A$ receptor activity by 3β-androstanediol, a neurosteroid predicted by our *in silico* metabolic reconstructions to be synthesized by PNEC cells, and known to be produced by androgen-refractory prostate tumors (21) (Fig. 3*D*). LNCaP cells did not respond to GABA, glycine, kainate, or NMDA, indicating that they do not express functional $GABA_A$, glycine, or glutamate receptors ($n = 6$, data not shown).

PNEC cells resemble neural progenitor cells when grown without attachment to substrates (8). Although $GABA_A$ receptor stimulation in differentiated neurons is inhibitory, receptor activation in neural progenitors is excitatory (22): this stems from the ability of these progenitor cells to maintain a relatively high intracellular chloride concentration, i.e., efflux of chloride ions through the $GABA_A$ receptor results in cell depolarization.

We used ratiometric calcium imaging to determine whether the effect of chloride channel stimulation by GABA and glycine was excitatory or inhibitory to PNEC cells. This method was used because (*i*) invasive electrophysiological recordings might disrupt ion gradients that form across the cell membrane and (*ii*) if membranes were depolarized in response to receptor stimulation, this may activate voltage sensitive Ca^{2+} channels, allowing the influx of Ca^{2+}. The results revealed that $GABA_A$, glycine, and glutamate receptor activation depolarize PNEC cells and increase their cytoplasmic Ca^{2+} levels (Fig. 3 *E* and *F* and Table 1, which is published as supporting information on the PNAS web site). Propylene glycol had no demonstrable effect on calcium influx at concentrations up to 1 mM (data not shown).

We then investigated the effect of GABA, glycine, and glutamate receptor antagonists on cell proliferation. Application of 100 μM picrotoxin ($GABA_A$ receptor antagonist), 1 μM strychnine (glycine receptor antagonist), or 10 μM NBQX (glutamate receptor antagonist) to PNEC neurospheres failed to affect cell proliferation. However, a combination of picrotoxin, strychnine, and NBQX inhibited proliferation by 30% compared to untreated controls ($n = 6$ replicates; $P < 0.005$). In contrast, 100 μM 2-hydroxysaclofen, a $GABA_B$ receptor antagonist, had no effect on proliferation, either by itself or in combination with picrotoxin. Furthermore, it did not significantly alter the inhibitory effect of combined treatment with picrotoxin, strychnine, and NBQX.

A Metabolome-Directed Therapeutic Regimen for NE Cancers. Abp1, which is involved in PNEC metabolic pathways that convert putrescine to GABA, histidine to the $GABA_A$ receptor agonist, imidazole-4-acetate (23) (Fig. 5), and glycine to propylene glycol, is inhibited by the diuretic amiloride (24). Dopa decarboxylase, which operates "upstream" of Abp1 in aromatic amine

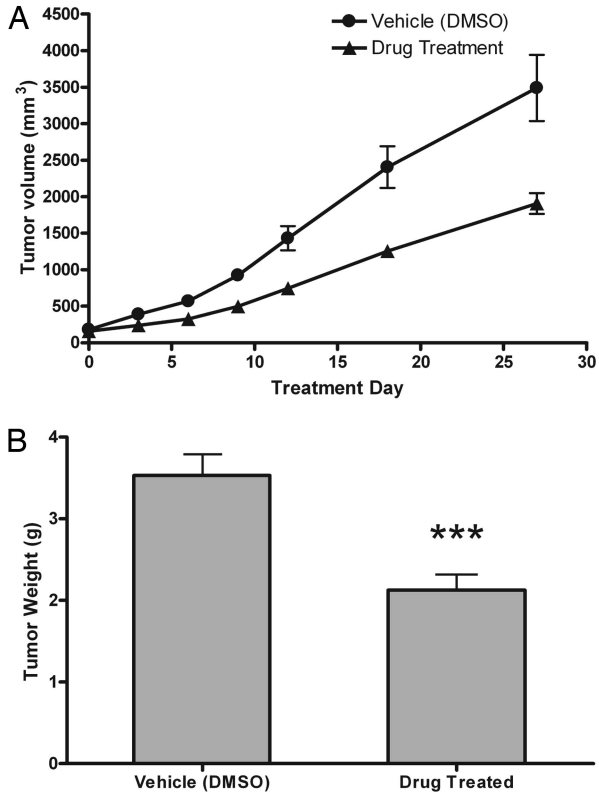

Fig. 4. Treatment of PNEC tumor-bearing mice. (*A*) Plot of PNEC tumor growth over treatment period. Tumor volume was estimated by using calipers and the formula $0.5W^2L$. The treatment group received daily injections of 100 mg/kg carbidopa, 20 mg/kg amiloride, and 10 mg/kg flumazenil in 20% DMSO. The control group received 20% DMSO alone ($n = 5$ animals per group; eight tumors total in vehicle-treated group, 10 tumors total in drug-treated group; mean values ± 1 SD are plotted). (*B*) Weight of tumors recovered from mice killed on day 30 of therapy. Asterisks represent significantly lower ($P < 0.0005$) tumor mass in the drug-treated group.

metabolism (Fig. 5), is inhibited by carbidopa, a drug routinely administered to patients with Parkinson's disease (25). Flumazenil, a benzodiazepine antagonist that binds to $GABA_A$ receptors, is used to reverse the effects of sedatives (26).

We examined whether a mixture of these drugs could inhibit growth of PNEC cells that had been implanted into nude mice and allowed to grow for 2 weeks before initiation of "pharmacometabolomic" therapy. Daily i.p. administration of 100 mg/kg carbidopa, 20 mg/kg amiloride, and 10 mg/kg flumazenil for 30 days produced a statistically significant 40% reduction in tumor growth ($P < 0.0005$ compared to vehicle-treated mice; $n = 10$ tumors/treated group, $n = 8$ tumors per vehicle group; Fig. 4 *A* and *B*). Interestingly, reduced tumor growth correlated with diminished SSADH activity [355 ± 14.1 pmol of succinate per μg of protein per h (treated, $n = 5$) versus 392.5 ± 9.7 (untreated, $n = 5$), $P < 0.05$].

Prospectus. Together, these findings suggest a treatment regimen for NE carcinomas, and possibly other cancers. Fig. 6, which is published as supporting information on the PNAS web site, shows results from Affymetrix GeneChip data sets, obtained from 471 NE and non-NE human cancers, that examine expression of transcripts encoding the GABA biosynthetic pathway enzymes ODC1, ABP1, ALDH9A1, and GAD1. One-way ANOVA statistical analyses revealed statistically significant enrichment in ABP1 expression in metastatic medullary thyroid carcinomas, lung adenocarcinomas with NED, as well as colon

and renal cell carcinomas, compared with other cancers ($P < 0.001$; see Tables 2–7, which are published as supporting information on the PNAS web site, for the sources of these GeneChip data sets and details about the results of the statistical analysis). Although glioblastoma multiforme (GBM) and anaplastic oligodendroglioma tumors of the central nervous system did not display detectable ABP1 expression, a statistically significant enrichment in GAD1 expression ($P < 0.0001$) was evident. Moreover, a recent report indicated that extracellular GABA concentrations in human glioma tumor tissue are significantly elevated compared to normal tissue and positively correlate with tumor grade (27).

Unfortunately, we were not able to correlate levels of ABP1 or GAD1 expression in these tumors with clinical outcome because the sample size was too small and/or because there was no patient information associated with the GeneChip data sets. Nonetheless, these observations indicate that future studies are needed to determine whether serum or tumor cell GABA concentrations are either predictive of aggressive cancer, useful for monitoring responses to existing therapeutic regimens, and/or an indication for clinical trials that use the type of "off the shelf" pharmacometabolomic therapy described in this report.

Materials and Methods

MAS-NMR Spectroscopy. Cell lines and tumors were snap-frozen in liquid N_2 immediately after they were harvested, freeze-dried at −35°C for 3–5 days, and then weighed. Samples were placed in a 50-μl-capacity glass rotor with a Teflon endcap and solvated with 40 μl of a standard solution of 2,2-dimethyl-2-silapentane-3,3,4,4,5,5-d_6-5-sulfonate sodium salt (DSS; Chenomx, Edmonton, Canada). NMR spectra were recorded on a Varian INOVA, 14.1 Tesla NMR spectrometer at a ^{1}H frequency of 600 MHz using a gHX nanoprobe. Magic angle spinning was regulated at 1,800 Hz for all experiments. ^{1}H NMR spectra were acquired by using the first slice of a NOESY experiment with a 1-s presaturation delay to suppress the residual water signal. Saturation was also used during the 200-ms NOESY mixing time. Acquisition time was 4 s, with no delay time between pulses, giving a total interpulse delay of 5 s. Assignments were made by using a combination of Chenomx profiler software and 2D HMQC, COSY, and TOCSY experiments. Using the MATLAB software computing environment (www.mathworks.com), spectra were normalized to have an area of 1, followed by the computation of mean and median spectra. MAS-NMR data sets are available at http://gordonlab.wustl.edu/metaview/ippolito.

Prediction of GABA Biotransformations. The structure of GABA was imported into the program METEOR (Lhasa, Leeds, U.K.) and queried against its database of phase I and phase II biotransformations. The "depth first search" method was used to obtain a list of all potential transformations of GABA. Masses and identities corresponding to the predicted transformations were queried against mass spectrometry data sets reported in ref. 8 and MAS–NMR data sets.

Pharmacometabolomic Studies. PNEC cells (10×10^7) were injected into each flank of 10 4- to 6-week-old nude mice. Two weeks later, animals were divided into two groups ($n = 5$ per group). A mixture of carbidopa, flumazenil, and amiloride (Sigma, St. Louis, MO) was prepared by dissolving the compounds in DMSO (Sigma). The solution was diluted in PBS to a final concentration of 20% DMSO, sterilized through a 0.2-μm polyethersulfone filter (Whatman, Middlesex, U.K.), and injected intraperitoneally into one group of mice (carbidopa, 100 mg per kg of body weight; amiloride, 20 mg/kg; flumazenil, 10 mg/kg). A vehicle consisting of 20% DMSO in PBS was injected into the second (control) group. Injections were performed every 24 h for 1 month. Tumors were measured periodically with calipers, and tumor volume was estimated by using the formula $0.5W^2L$. The area under the growth curve for each tumor was calculated, and data from the two groups of mice were compared by using the two-tailed t test in Prism software (GraphPad, San Diego, CA). Tumors were harvested at the time of death and weighed.

For further details, see *Supporting Text*, which is published as supporting information on the PNAS web site.

We thank Sabrina Wagoner, Dave O'Donnell, Maria Karlsson, Kristin Bullok, Marios Giannakis, Jeffrey Milbrandt, Jeffrey Arbeit, Garret Hampton, and Charles Powell for valuable assistance. This work was funded by National Institutes of Health Grants DK59129, DK63483, CA94056, RR00954, AA12952, and DA18109, and American Cancer Society Grant IRG-58-010-49, and is dedicated to Americo Ippolito.

1. Manger, W. M. & Gifford, R. W. (1995) in *Hypertension: Pathophysiology, Diagnosis, and Management*, ed. Laragh, J. H. & Brenner, B. M. (Raven, New York), pp. 2225–2244.
2. Sorensen, M., Lassen, U. & Hansen, H. H. (1998) *Curr. Opin. Oncol.* **10,** 133–138.
3. Eren, F., Celikel, C. & Gulluoglu, B. (2004) *Pathol. Oncol. Res.* **10,** 47–51.
4. Shinji, S., Naito, Z., Ishiwata, T., Tanaka, N., Furukawa, K., Suzuki, H., Seya, T., Kan, H., Tsuruta, H., Matsumoto, S., *et al.* (2006) *Int. J. Oncol.* **29,** 357–364.
5. Quek, M. L., Daneshmand, S., Rodrigo, S., Cai, J., Dorff, T. B., Groshen, S., Skinner, D. G., Lieskovsky, G. & Pinski, J. (2006) *Urology* **67,** 1247–1252.
6. Abrahamsson, P. A. (1999) *Prostate* **39,** 135–148.
7. Bhattacharjee, A., Richards, W. G., Staunton, J., Li, C., Monti, S., Vasa, P., Ladd, C., Beheshti, J., Bueno, R., Gillette, M., *et al.* (2001) *Proc. Natl. Acad. Sci. USA* **98,** 13790–13795.
8. Ippolito, J. E., Xu, J., Jain, S., Moulder, K., Mennerick, S., Crowley, J. R., Townsend, R. R. & Gordon, J. I. (2005) *Proc. Natl. Acad. Sci. USA* **102,** 9901–9906.
9. Garabedian, E. M., Humphrey, P. A. & Gordon, J. I. (1998) *Proc. Natl. Acad. Sci. USA* **95,** 15382–15387.
10. Hu, Y., Ippolito, J. E., Garabedian, E. M., Humphrey, P. A. & Gordon, J. I. (2002) *J. Biol. Chem.* **277,** 44462–44474.
11. Hu, Y., Wang, T., Stormo, G. D. & Gordon, J. I. (2004) *Proc. Natl. Acad. Sci. USA* **101,** 5559–5564.
12. Horoszewicz, J. S., Leong, S. S., Kawinski, E., Karr, J. P., Rosenthal, H., Chu, T. M., Mirand, E. A. & Murphy, G. P. (1983) *Cancer Res.* **43,** 1809–1818.
13. Griffin, J. L. (2003) *Curr. Opin. Chem. Biol.* **7,** 648–654.
14. Becker, E. D. (2000) *High Resolution NMR: Theory and Chemical Applications* (Academic, London).
15. Xu, D., Dhillon, A. S., Abelmann, A., Croft, K., Peters, T. J. & Palmer, T. N. (1998) *Metabolism* **47,** 1180–1186.
16. Lomeo, F., Khokher, M. A. & Dandona, P. (1988) *Diabetes* **37,** 912–915.
17. Shelp, B. J., Bown, A. W. & McLean, M. D. (1999) *Trends Plant Sci.* **4,** 446–452.
18. Yogeeswari, P., Sriram, D. & Vaigundaragavendran, J. (2005) *Curr. Drug. Metab.* **6,** 127–139.
19. Greenberg, N. M., DeMayo, F., Finegold, M. J., Medina, D., Tilley, W. D., Aspinall, J. O., Cunha, G. R., Donjacour, A. A., Matusik, R. J. & Rosen, J. M. (1995) *Proc. Natl. Acad. Sci. USA* **92,** 3439–3443.
20. Nakanishi, S. (1992) *Science* **258,** 597–603.
21. Harkonen, P., Torn, S., Kurkela, R., Porvari, K., Pulkka, A., Lindfors, A., Isomaa, V. & Vihko, P. (2003) *J. Clin. Endocrinol. Metab.* **88,** 705–712.
22. Wang, D. D., Krueger, D. D. & Bordey, A. (2003) *J. Physiol.* **550,** 785–800.
23. Fogel, W. A., Bieganski, T., Bechtold, E. & Maslinski, C. (1982) *Agents Actions* **12,** 49–52.
24. Novotny, W. F., Chassande, O., Baker, M., Lazdunski, M. & Barbry, P. (1994) *J. Biol. Chem.* **269,** 9921–9925.
25. Burkhard, P., Dominici, P., Borri-Voltattorni, C., Jansonius, J. N. & Malashkevich, V. N. (2001) *Nat. Struct. Biol.* **8,** 963–967.
26. Zheng, T. M., Caruncho, H. J., Zhu, W. J., Vicini, S., Ikonomovic, S., Grayson, D. R. & Costa, E. (1996) *J. Pharmacol. Exp. Ther.* **277,** 525–533.
27. Bianchi, L., De Micheli, E., Bricolo, A., Ballini, C., Fattori, M., Venturi, C., Pedata, F., Tipton, K. F. & Della Corte, L. (2004) *Neurochem. Res.* **29,** 325–334.